Sensors & Actuators: B. Chemical 296 (2019) 126615

Contents lists available at ScienceDirect

Sensors and Actuators B: Chemical

journal homepage: www.elsevier.com/locate/snb

Microfluidic multiple cross-correlated Coulter counter for improved particle size analysis

Wenchang Zhang[a,1], Yuan Hu[a,1], Gihoon Choi[b], Shengfa Liang[a], Ming Liu[a,**], Weihua Guan[b,c,*]

[a] Key Lab of Microelectronic Devices & Integrated Technology, Institute of Microelectronics, Chinese Academy of Sciences, Beijing, 100029, China
[b] Department of Electrical Engineering, Pennsylvania State University, University Park, 16802, USA
[c] Department of Biomedical Engineering, Pennsylvania State University, University Park, 16802, USA

ARTICLE INFO

Keywords:
Coulter counter
Particle sizing
Resistive pulse sensors
Multiple cross-correlation analysis

ABSTRACT

Coulter counters (a.k.a. resistive pulse sensors) were widely used to measure the size of biological cells and colloidal particles. One of the important parameters of Coulter counters is its size discriminative capability. This work reports a multiple pore-based microfluidic Coulter counter for improved size differentiation in a mixed sample. When a single particle translocated across an array of sensing pores, multiple time-related resistive pulse signals were generated. Due to the time correlation of these resistive pulse signals, we found a multiple cross-correlation analysis (MCCA) could enhance the sizing signal-to-noise (*SNR*) ratio by a factor of $n^{1/2}$, where n is the pore numbers in series. This proof-of-concept is experimentally validated with polystyrene beads as well as human red blood cells. We anticipate this method would be highly beneficial for applications where improved size differentiation is required.

1. Introduction

Coulter counters, also known as the resistive pulse sensors, are well-developed devices to measure the size and concentration of biological cells and colloidal particles suspended in a buffer solution [1–5]. In Coulter devices, including its microfluidic versions, two electrolyte-filled compartments or chambers are separated by a microscopic conduction path. When a particle flows through this orifice, the device electrical resistance is temporarily changed. This resistance change is often measured as a current dip, the magnitude and the duration of which is correlated to size, shape, mobility, surface charge and concentration of the particles [6–13]. Due to its simplicity and reliability, the resistive pulse sensor has been used for a variety of applications [14–25], ranging from the analysis of blood cells [15,18,19,22] to the detection and counting of colloidal beads [25], pollen [14], and viruses [24]. In addition, nanoscale Coulter counter devices such as nanopores [26–30], was also developed to detect proteins [26,27], and DNAs [28].

One important parameter of the Coulter counter devices is their size discriminative capability [1,3,11,13,16,31,32]. A better size differentiation ability means particles of different sizes can be counted more accurately and the misclassification rate can be reduced. Since the particle size is inferred from the resistance change when particles translocating through the pore, sizing ability is highly dependent on the precise detection of the current dip magnitude, and the volume ratio of the particle to the sensing pore [11,20,31–34]. Existing approaches for improving the sizing precision were dominated by reducing the volume ratio of the particle to the sensing pore. For example, hydrodynamic focusing was adopted by flowing a conductive sample liquid between parallel nonconductive sheath liquid [35,36]. By doing so, the effective pore size can be reduced by adjusting the flow rate ratio between sample and sheath liquid. Another example is to adopt a mechanically tunable sensing pore [37–39] such that the size would be dynamically controlled, allowing for the detection of a widely distributed particle size.

In this work, we presented an alternative approach for improving the size differential capability of microfluidic Coulter Counter. This is achieved by passing particles through multiple pores in series such that each particle is detected multiple times by these sequential pores. The current dip generated were analyzed by multiple cross-correlation analysis (MCCA). The basic principle to increase the sizing differential capability relies on the fact that the sequential current dip signals are correlated in the time domain, while the noise is not. The MCCA method greatly enhances the *SNR* of the sizing capability. This enhancement could significantly improve sizing precision and reduce the

* Corresponding author at: Department of Electrical Engineering, Pennsylvania State University, University Park, 16802, USA.
** Corresponding author.
E-mail addresses: liuming@ime.ac.cn (M. Liu), w.guan@psu.edu (W. Guan).
[1] The authors contributed equally.

https://doi.org/10.1016/j.snb.2019.05.092
Received 4 January 2019; Received in revised form 22 April 2019; Accepted 25 May 2019
Available online 29 May 2019
0925-4005/

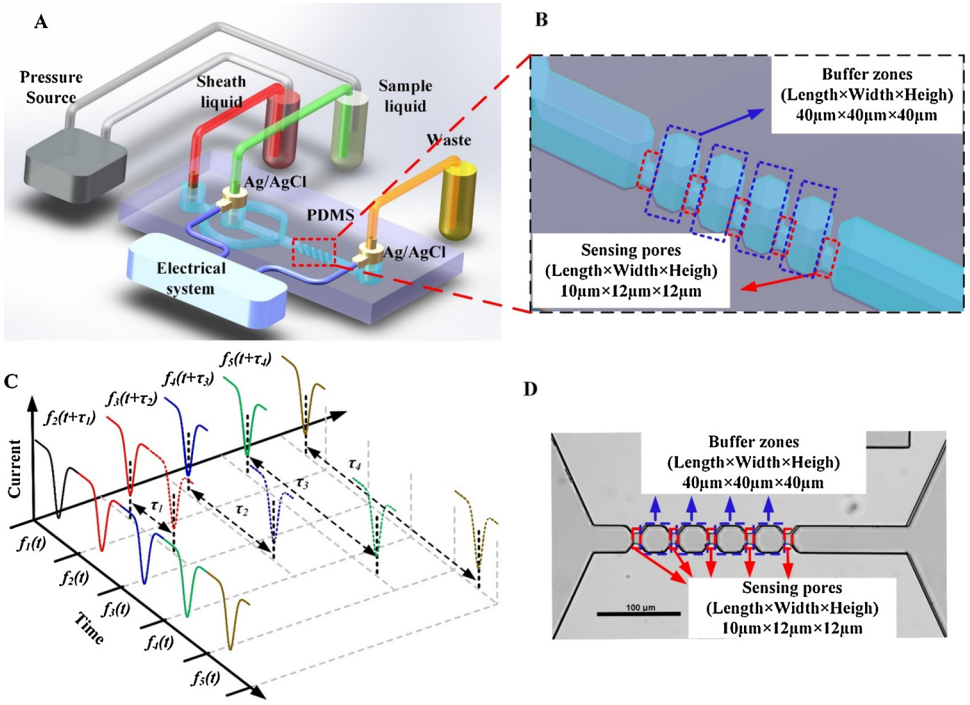

Fig. 1. (A) The principle of multiple sensing pores for improved size discrimination. A pair of Ag/AgCl electrodes are plugged into the tubes of sample liquid and waste to apply a voltage signal and measure current change. A signal with multiple drop pulses is generated when a particle passing through sensing pores sequentially. (B) Enlarged schematic diagram of sequent sensing pores (10 μm × 12 μm × 12 μm). The buffer zones (40 μm × 40 μm × 40 μm) are for separating the five current dip pulses of the sensing pores. (C) Schematic of multiple cross-correlation analysis. (D) Bright field image of the multiple sensing pores.

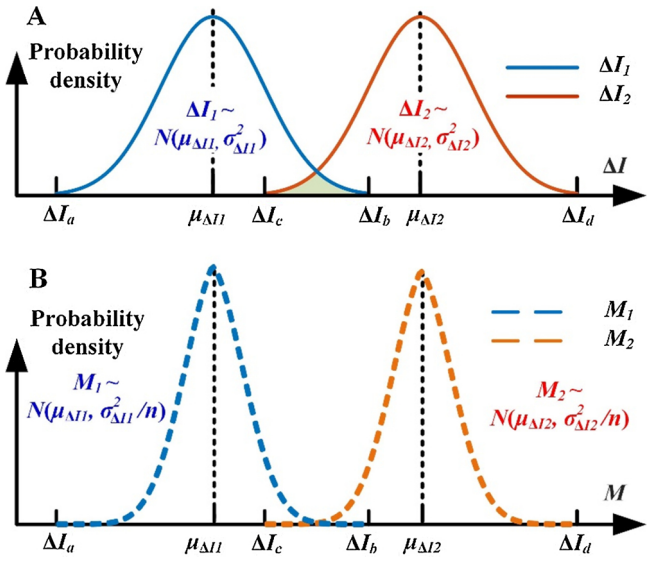

Fig. 2. Schematic diagram of the probability density distribution of (A) current dip Δ*I*, and (B) *M* values from MCCA method. The overlapped rate could be defined as the area of the dark region.

misclassification rate. We experimentally validated this approach with model beads and cells. We anticipate this approach could be extended to a variety of applications where sizing precision is needed.

2. Materials and methods

2.1. Chemicals and materials

SU-8 negative photoresists (SU8-2010, SU8-2025) were purchased from Rdmicro Corp (Suzhou, China). Photoresist-developing reagent SU-8 Developer (Microchem) was provided by the Rdmicro Corp (Suzhou, China). Silver wire (diameter 0.25 mm, ≥99.99% trace metals basis) and Potassium chloride (KCl, assay ≥99%) were purchased from Sigma-Aldrich Corp (Shanghai, China). Phosphate-buffered saline (PBS) (1×) were obtained from Macklin Corp (Shanghai, China), and Tween-20 was purchased from ThermoFisher Scientific Corp (Shanghai, China). Polystyrene beads (density 1.05 g/cm^3, refractive index 1.59): PS6000 solution (6.0 μm, PS8000 solution (8.0 μm), PS8500 solution (8.5 μm), PS9000 solution (9.0 μm) and PS10000 solution (10.0 μm) were provided by Smartynano technology Corp (Suzhou, China). The coefficients of variation (CVs) of all the polystyrene beads are < 3.5%, and the bead concentration is 5%. Human red blood cells (RBCs) (concentration 5%) was purchased from Gaining Biological (Shanghai, China).

2.2. Device design and fabrication

The Coulter counter with multiple sensing pores was designed in a layout editor and printed on a transparent mask. The casting mold was fabricated by a standard double-layer lithography process on a 4-inch silicon wafer. The microfluidic chip was made of polydimethylsiloxane (PDMS) by casting onto the SU8 mold. It consists of two layers with different thicknesses: micropores area with ~12 μm and buffer zones with ~40 μm, respectively. The thickness of the loading channel area is the same as that of buffer zones. To avoid the micropore clogging by particle aggregates and debris, one stage of filters was incorporated on the microfluidic chip in the loading channel area. The micropore width needs to be small enough for improved signal-to-noise ratio but also large enough for avoiding clogging. 12 μm was selected as the optimized width for the experiments. The length of the micropores (~10 μm) also needs to be optimized. A longer channel makes the pulse width larger, making the multiple pulses more recognizable, while a longer channel increases the risk of clogging. The PDMS replica was permanently bonded to the cover glass (thickness ~130 μm, Ted Pella) through oxygen plasma treatment. AgCl was coated on Ag wire by deposition in KCl solution with Pt as a reference electrode to fabricate the Ag/AgCl electrodes. A pair of Ag/AgCl electrodes were then inserted into the tubes of sample liquid and waste for DC excitation and current change detection. Ag/AgCl electrodes were connected to the electrical system for current amplification and current/voltage conversion.

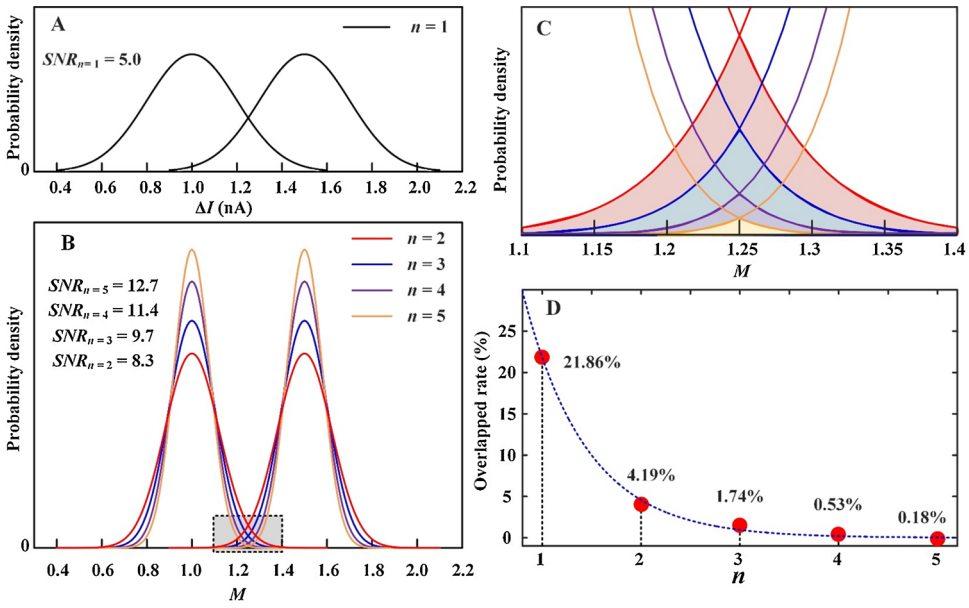

Fig. 3. Improvement of *SNR* by multiple sensing pores. The simulation is performed with $\mu_{\Delta I_1} = 1.0$ nA and $\sigma_{\Delta I_1} = 0.2$ nA, and $\mu_{\Delta I_2} = 1.5$ nA and $\sigma_{\Delta I_2} = 0.2$ nA. (A) The probability density of ΔI with 99.73% confidence bounds $\mu_{\Delta I} \pm 3\sigma_{\Delta I}$. (B) *SNR* for various sensing pore numbers (n = 2, 3, 4, 5). (C) Enlarged view of the overlapped region (dark area in Fig. 3B). (D) Quantitative results of overlapped rates.

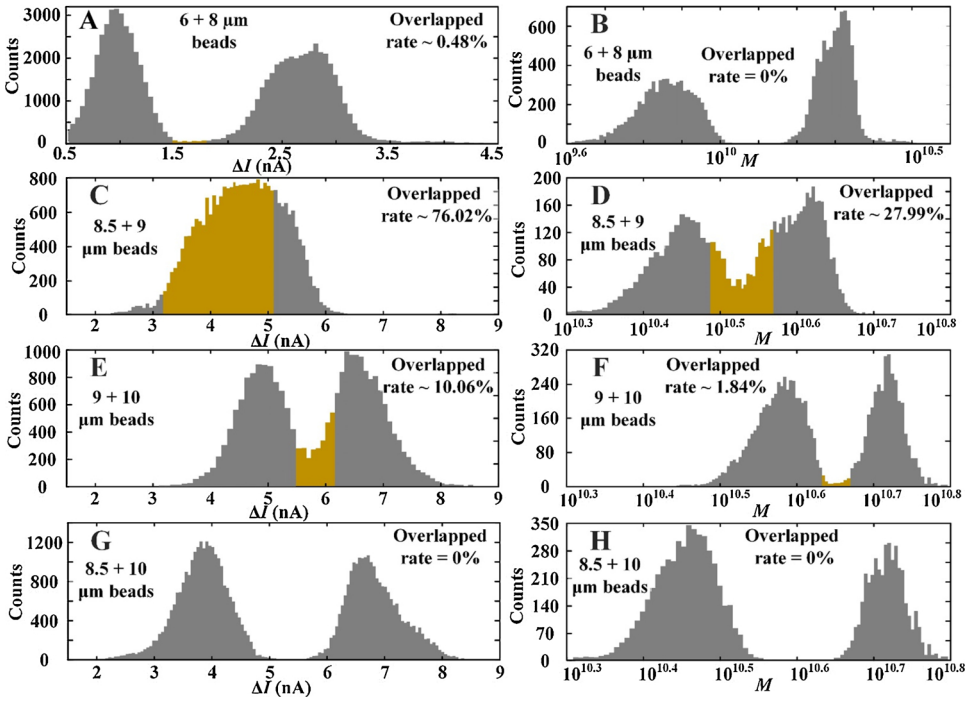

Fig. 4. Improvement of bead size differentiation capability by MCCA method. (A)-(B) 6 μm + 8 μm, (C)-(D) 8.5 μm + 9 μm, (*E*)-(F) 9 μm + 10 μm, and (G)-(H), 8.5 μm + 10 μm. The left panels are ΔI distribution, the right panels are M value distribution.

2.3. Sample preparation

For the analysis of same type particles, the suspension was prepared by mixing 30 μl sample solution (PS6000, PS8000, PS8500, PS9000, PS10000, RBCs solution) with 3 ml 1 × PBS respectively. The mixture suspension of 6 μm and 8 μm beads was prepared by mixing 15 μl PS6000 solution and 15 μl PS8000 with 3 ml 1 × PBS; the mixture suspension of 8.5 μm and 9 μm beads was prepared by mixing 15 μl PS8500 solution and 15 μl PS9000 with 3 ml 1 × PBS; the mixture suspension of 8.5 μm and 10 μm beads was prepared by mixing 15 μl PS8500 solution and 15 μl PS10000 with 3 ml 1 × PBS; the mixture suspension of 9 μm and 10 μm beads was prepared by mixing 15 μl PS9000 solution and 15 μl PS10000 with 3 ml 1 × PBS; the mixture suspension of RBCs and 8 μm beads was prepared by mixing 15 μl RBCs solution and 15 μl PS8000 with 3 ml 1 × PBS. All the suspensions were added with 0.1% Tween-20 to avoid bead aggregation and oscillated with an ultrasonic cleaner for 1 min to achieve better monodisperse situation. In particular, the 1x PBS was also used as sheath liquid.

2.4. Electrical measurement and data analysis

After device fabrication, the microfluidic chip was housed inside a

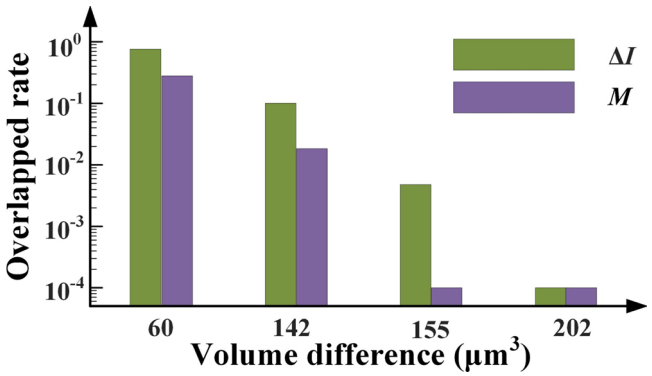

Fig. 5. Overlapped rates with ΔI and M as the criterion for various size mixtures.

home-made Faraday cage to shield the environment noise. Sheath fluid is used to form laminar flow and restrict the location of particles suspended in the sample fluid. The flow rates of sheath and sample liquid are controlled by a pressure source. In a typical experiment, a pressure of 0.3– 0.5 psi is applied. A constant voltage (˜200 mV) was applied across the microchannel constriction. The ionic current was monitored as individual particles translocating through the sensing pores. The ionic current traces were amplified and converted to a voltage signal by an amplifier (DHPCA-100, Femto, Germany). The analog voltage output of the amplifier was sampled with 16-bit DAQ card (NI PCI-6363, National Instruments, USA) and a data acquisition software (LabVIEW). The sampling rate for the measurement was 100 kHz. A custom-built MATLAB (MathWorks) program was developed to analyze the data offline.

Fig. 1 shows the principle of microfluidic Coulter counter with multiple sensing pores (five pores as an example). When the single particle flows through sequential micropores on the microfluidic chip, a current signal with multiple time-correlated dips is generated. The principle of MCCA is schematically shown in Fig. 1C. The dip pulses of one particle could be extracted to five individual pulses $f_i(t)$ (i = 1, …, 5) with simple signal processing for MCCA.

3. Results and discussion

3.1. Working principle

For conventional single-pore based Coulter counter, the current dip (denoted by ΔI) is proportional to the particle size [6]. Due to the measurement noise, the ΔI distribution could be well modeled by a Gaussian distribution [4], $\Delta I \sim N(\mu_{\Delta I}, \sigma^2_{\Delta I})$, in which $\mu_{\Delta I}$ is the mean value of the current dip and$\sigma_{\Delta I}$ is the standard deviation representing the measurement uncertainty. Assuming no particle size variations, the uncertainty of ΔI is mainly from the electrical measurement. This broadening of the ΔI due to the measurement uncertainty contributes to the deterioration of the particle sizing classification. If we have a mixed sample containing two different particle size, the expected current dip from each population is thus $\Delta I_1 \sim N(\mu_{\Delta I1}, \sigma^2_{\Delta I1})$ and $\Delta I_2 \sim N(\mu_{\Delta I2}, \sigma^2_{\Delta I2})$. The broadening of the ΔI from each population would results in the overlapping of ΔI distribution (Fig. 2A) and negatively impact the particle size distinguishability. Two approaches could be adopted to eliminate the ΔI overlapping: one is to expand the distance between the mean value ($\mu_{\Delta I2} - \mu_{\Delta I1}$), the other is to reduce the measurement variations ($\sigma_{\Delta I1}$ and$\sigma_{\Delta I2}$). We define an *SNR* parameter as μ/σ. It is clear higher *SNR* would mean better size differentiation.

Considering microfluidic Coulter counter with n pores, multiple dip pulses $f_i(t)$ (i = 1, …, n) with a DC baseline I_{DC} are generated as particles translocating through each pore. Performing a cross-correlation analysis of $f_i(t)$, the resulting maximum value of the alternating component is (see supplementary information for details)

$$M \approx \sqrt{2\pi} I_{DC}^{(n-1)} \sigma \sum_{i=1}^{n} \Delta I_i \tag{1}$$

where ΔI_i (i = 1, …, n) is the magnitude of each current dip, and σ represents the pulse width. According to Eq. 1 and the distribution character of ΔI, we conclude that M also follows a Gaussian distribution with a mean of $\sqrt{2\pi} I_{DC}^{(n-1)} \sigma n \mu_{\Delta I}$and a standard deviation of $\sqrt{2\pi} I_{DC}^{(n-1)} \sigma \sqrt{n} \sigma_{\Delta I}$ (see supplementary information for details). As a result, the *SNR* of n-pores is

$$SNR(M) = \sqrt{n} \cdot SNR(\Delta I) \tag{2}$$

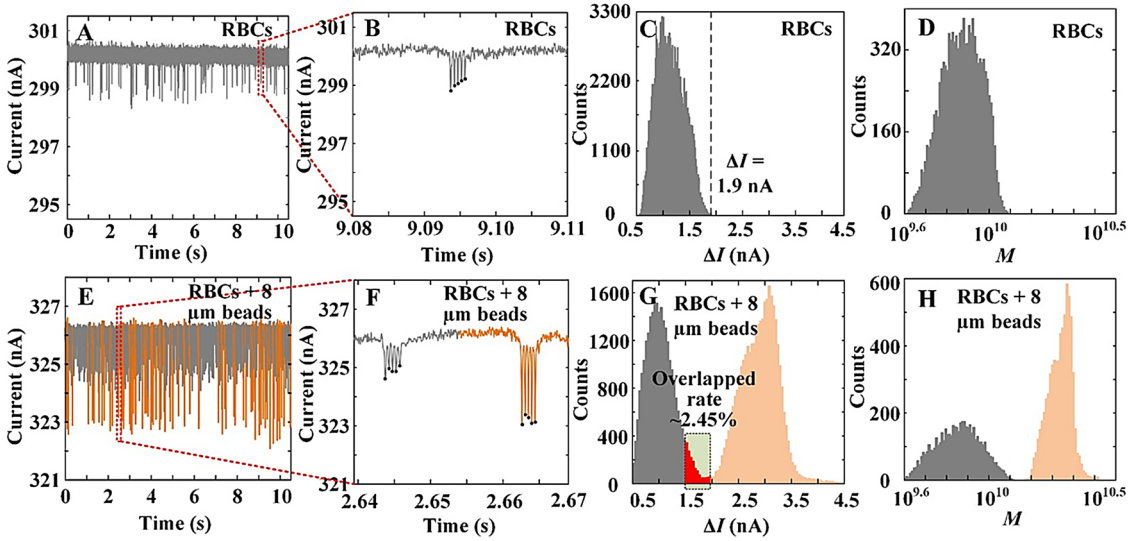

Fig. 6. (A) Time series of the current profile measured within 10.5 s with RBCs passing through. (B) One of the enlarged five pulse signals of the profile circled in (A). (C) Histogram of ΔI of 11,830 events (RBCs). (D) Histogram of M of 11,830 events (RBCs). (E) Time series of the current profile measured within 10.5 s with RBCs + 8um polystyrene beads passing through. (F) Two of the enlarged five pulse signals of the profile circled in (E). (G) Histogram of ΔI of 12,849 events (RBCs + 8 μm) with overlapped rate of 2.45%. (H) Histogram of M of 12,849 events (RBCs + 8 μm) with overlapped rate of 0%.

It is clear that the *SNR* could be amplified with the MCCA method by the gain of $\sqrt{n}$. In order to visualize the *SNR* improvement, the *M* distribution is scaled and overlaid to the ΔI distribution (Fig. 2B). It is clear the distribution overlap is much reduced with this proposed MCCA method, *i.e.,* the size differentiation could be greatly improved. It is clear from Eq. 2 that this improvement has a tradeoff with the analyzing throughput.

3.2. Improvement of SNR by multiple sensing pores

In order to analyze the *SNR* improvement with different numbers of sensing pores, we performed a simulation with overlapped ΔI distributions. The results of sensing pores ranging from 2 to 5 are shown in Fig. 3B. *SNR* increases from 5.0 to 12.7 as the number of pores *n* increases from 1 to 5, and the overlapped region is greatly reduced. Fig. 3C shows the enlarged view of the overlapped region in Fig. 3B (dark area) while Fig. 3D shows the quantitative results. The overlapped rate decreases significantly (from 21.86% down to 0.18%) with MCCA when the pore number increases from 1 to 5. While increasing the pore numbers would increase the *SNR*, it is clear from Fig. 3D that the benefits would diminish when *n* is sufficiently large. Considering the analyzing throughput, we conclude that $n = 5$ would be optimized for experiments (less than 0.2% overlap).

3.3. Validation

Based on the above analysis and simulation, experiments using different polystyrene bead mixtures were performed. Before the mixture experiments, individual sized polystyrene beads were tested separately to verify the microfluidic chip and detection system (See Supplementary Figure S1 for current time traces and histograms of ΔI and *M*). For the mixture sample, various combinations were tested (Fig. 4). Fig. 4A and B shows the results from a mixture sample of 6 μm and 8 μm beads. A total number of 15,124 events were collected for statistical analysis (sensing throughput ~1600 events/min). The improvement of size classification is apparent by evaluating the overlapped rate. With ΔI as a criterion (Fig. 4A), the events between 1.5 nA and 1.8 nA cannot be classified precisely, the overlapped rate is ~0.48%. While as for the MCCA method (Fig. 4B), no overlapping was observed between subpopulations. The ΔI overlap in Fig. 4A is more likely introduced by the measurement errors, rather than the bead size variation. Since the *M* value (Eq.1) is from five consecutive measurements, *M* value is more noise-robust, *i.e.*, the current dip measurement error from a single pore would not seriously deteriorate the *M* value.

This same improvement of size differentiation capability was also observed for other mixtures with different size. Fig. 4C-H show the histograms of ΔI and *M* from these experiments (sensing throughput ~1600 events/min). As shown in Fig. 4C, there is severe overlap (76.02%) in the ΔI histogram if the particle volume difference is too small (8.5 μm *versus* 9 μm). In this case, the overlapped rate is decreased significantly to 27.99% with MCCA method (Fig. 4D). Fig. 5 summarizes the overlapped rate in both methods for all mixture combinations we tested. It is clear that the overlapped rate could be significantly reduced with MCCA, and the minimum particle volume difference could be recognized is much smaller than that of ΔI.

To validate the MCCA method for cells, we first characterized the human RBCs alone (Fig. 6A-D). The time traces were shown in Fig. 6A, where the five dips were apparent in the explored view (Fig. 6B). Fig. 6C shows the ΔI distribution for a total of 11,830 events, whereas Fig. 6D shows the MCCA result. After this evaluation, we went on to analyze the human RBCs with 8 μm bead as a background population (sensing throughput ~1800 events/min). Fig. 6E-H show the testing result. A total of 12,849 events were detected for the statistical analysis. The overlapped rate between the RBCs and the beads is ~2.45% with ΔI as the criterion (Fig. 6G), which was greatly reduced to 0% by using the MCCA method (Fig. 6H).

4. Conclusion

A microfluidic Coulter counter based on multiple sensing pores has been developed to improve the sizing precision. A single particle is detected more than once, and the multiple time-related pulses are analyzed with MCCA. It is found that the sizing *SNR* would be amplified by $\sqrt{n}$, where *n* is the number of sensing pores. We have successfully demonstrated this concept by testing model beads and human RBCs. Multiple cross-correlation analysis greatly reduces the overlapped rate and misclassification of subpopulation size. While the analysis throughput could be negatively impacted by multiple sensing pore, the random fluctuation error in the single micropore could be alleviated by the correlated signals from the multiple sensing pores. We expect this proof-of-concept would be highly beneficial for applications where improved sizing discrimination capability is required.

Declarations of interest

None.

Acknowledgments

This project was partially supported by a grant from National Science Foundation, USA (ECCS-1710831) as well as China Postdoctoral Science Foundation (2017M620942), National Key R&D Program of China (2016YFB0402703) and National Key Scientific Instruments and Equipment Development Project of China (51727901).

Appendix A. Supplementary data

Supplementary material related to this article can be found, in the online version, at doi:https://doi.org/10.1016/j.snb.2019.05.092.

References

[1] R.W. Deblois, C.P. Bean, Counting and sizing of submicron particles by the resistive pulse technique, Rev. Sci. Instrum. 41 (1970) 909–916.
[2] C.M.L. Atkinson, R. Wilson, Artifact peaks in Particle-Size distributions measured by the electrical sensing zone (Coulter-Counter) method, Powder Technol. 34 (1983) 275–284.
[3] B.C. Marshall Don, Graham, the Coulter principle: foundation of an industry, J. Assoc. Lab. Autom. 8 (2003) 72–81.
[4] M.A. Mansor, M.R. Ahmad, Single cell electrical characterization techniques, Int. J. Mol. Sci. 16 (2015) 12686–12712.
[5] Y.C. Xu, X.W. Xie, Y. Duan, L. Wang, Z. Cheng, J. Cheng, A review of impedance measurements of whole cells, Biosens. Bioelectron. 77 (2016) 824–836.
[6] S. Gawad, L. Schild, P.H. Renaud, Micromachined impedance spectroscopy flow cytometer for cell analysis and particle sizing, Lab Chip 1 (2001) 76–82.
[7] N. Watkins, B.M. Venkatesan, M. Toner, W. Rodriguez, R. Bashir, A robust electrical microcytometer with 3-dimensional hydrofocusing, Lab Chip 9 (2009) 3177–3184.
[8] M. Nasir, D.A. Ateya, D. Burk, J.P. Golden, F.S. Ligler, Hydrodynamic focusing of conducting fluids for conductivity-based biosensors, Biosens. Bioelectron. 25 (2010) 1363–1369.
[9] D.P. Sun, J. Lu, Z.G. Chen, Microfluidic contactless conductivity cytometer for electrical cell sensing and counting, RSC Adv. 5 (2015) 59306–59313.
[10] S. Emaminejad, K.H. Paik, V. Tabard-Cossa, M. Javanmard, Portable cytometry using microscale electronic sensing, Sens. Actuator B Chem. 224 (2016) 275–281.
[11] D. Spencer, F. Caselli, P. Bisegna, H. Morgan, High accuracy particle analysis using sheathless microfluidic impedance cytometry, Lab Chip 16 (2016) 2467–2473.
[12] E.J. Garboczi, The influence of particle shape on the results of the electrical sensing zone method as explained by the particle intrinsic conductivity, Powder Technol. 322 (2017) 32–40.
[13] J. He, A.T. Brimmo, M.A. Qasaimeh, P. Chen, W. Chen, Recent advances and perspectives in microfluidics-based single-cell biosensing techniques, Small Methods 1 (2017) 1–19 1700192.
[14] J.Z. Zheng Zhang, Santanu Chandra, Jun Hu, An electronic pollen detection method using Coulter counting principle, Atmos. Environ. 39 (2005) 5446–5453.
[15] D. Holmes, D. Pettigrew, C.H. Reccius, J.D. Gwyer, C. van Berkel, J. Holloway, et al., Leukocyte analysis and differentiation using high speed microfluidic single cell impedance cytometry, Lab Chip 9 (2009) 2881–2889.
[16] S.Z. Hua, T. Pennell, A microfluidic chip for real-time studies of the volume of single cells, Lab Chip 9 (2009) 251–256.
[17] C. Bernabini, D. Holmes, H. Morgan, Micro-impedance cytometry for detection and analysis of micron-sized particles and bacteria, Lab Chip 11 (2011) 407–412.
[18] C. van Berkel, J.D. Gwyer, S. Deane, N.G. Green, J. Holloway, V. Hollis, et al.,

Integrated systems for rapid point of care (PoC) blood cell analysis, Lab Chip 11 (2011) 1249–1255.
[19] M. Evander, A.J. Ricco, J. Morser, G.T.A. Kovacs, L.L.K. Leung, L. Giovangrandi, Microfluidic impedance cytometer for platelet analysis, Lab Chip 13 (2013) 722–729.
[20] Y. Zheng, J. Nguyen, Y. Wei, Y. Sun, Recent advances in microfluidic techniques for single-cell biophysical characterization, Lab Chip 13 (2013) 2464–2483.
[21] R. Rodriguez-Trujillo, M.A. Ajine, A. Orzan, M.D. Mar, F. Larsen, C.H. Clausen, et al., Label-free protein detection using a microfluidic Coulter-counter device, Sens. Actuator B Chem. 190 (2014) 922–927.
[22] U. Hassan, B. Reddy Jr., G. Damhorst, O. Sonoiki, T. Ghonge, C. Yang, et al., A microfluidic biochip for complete blood cell counts at the point-of-care, Technology (Singap World Sci.) 3 (2015) 201–213.
[23] T.W. Murphy, Q. Zhang, L.B. Naler, S. Ma, C. Lu, Recent advances in the use of microfluidic technologies for single cell analysis, Analyst 143 (2018) 60–80.
[24] N.N. Watkins, U. Hassan, G. Damhorst, H.K. Ni, A. Vaid, W. Rodriguez, et al., Microfluidic CD4(+) and CD8(+) t lymphocyte counters for point-of-Care HIV diagnostics using whole blood, Sci. Transl. Med. 5 (2013) 1–11 214ra170.
[25] O.A.S. Saleh, L. Lydia, On-chip resistive sensing of sub-micron particles, American physical society, Annual March Meeting (2001).
[26] P. Waduge, R. Hu, P. Bandrakar, H. Yamazaki, B. Cressiot, Q. Zhao, P. Whitford, M. Wanunu, Nanopore-based measurements of protein size, fluctuations, and conformational changes, ACS Nano 11 (2017) 5706–5716.
[27] D.P. Hoogerheide, P.A. Gurnev, T.K. Rostovtseva, S.M. Bezrukov, Real-time nanopore-based recognition of protein translocation success, Biophys. J. 114 (2018) 772–776.
[28] M. Karolis, E. Niklas, U.F. Keyser, QuipuNet: convolutional neural network for single-molecule nanopore sensing, Nano Lett. 6 (2018) 4040–4045.
[29] L. Kidan, P. Kyeong-Beom, K. Hyung-Jun, Y. Jae-Seok, C. Hongsik, K. Hyun-Mi, et al., Recent progress in solid-state nanopores, Adv. Mater. 30 (2018) 1–28 1704680.
[30] Fa.Z. Rivas, K. Osama, Heidi Reesink, L. Peal, T. Bridgette, Nixon, J. Alan, Deangelis, L. Paul, Skardal, Aleksander, Rahbar, Elaheh, Hall, R. Adam, Label-free analysis of physiological hyaluronan size distribution with a solid-state nanopore sensor, Nat. Commun. 9 (1-9) (2018) 1037.
[31] N. Kubota, M. Kobari, I. Hirasawa, Analytical and numerical study of detector sensitivity and resolution effects on metastable zone width, Crystengcomm 15 (2013) 2091–2098.
[32] Y. Chen, S.J. Kim, J.H. Guo, Y.J. Kang, J.P. Kausalya, A.G.M. Ong, et al., Portable Coulter counter with vertical through-holes for high-throughput applications, Sens. Actuator B Chem. 213 (2015) 375–381.
[33] E.L.C.J. Blundell, L.J. Mayne, E.R. Billinge, M. Platt, Emergence of tunable resistive pulse sensing as a biosensor, Anal Methods-Uk 7 (2015) 7055–7066.
[34] H. Yasaki, T. Yasui, T. Yanagida, N. Kaji, M. Kanai, K. Nagashima, et al., Substantial expansion of detectable size range in ionic current sensing through pores by using a microfluidic bridge circuit, J. Am. Chem. Soc. 139 (2017) 14137–14142.
[35] J.H. Nieuwenhuis, F. Kohl, J. Bastemeijer, P.M. Sarro, M.J. Vellekoop, Integrated Coulter counter based on 2-dimensional liquid aperture control, Sens. Actuator B Chem. 102 (2004) 44–50.
[36] R. Rodriguez-Trujillo, O. Castillo-Fernandez, M. Garrido, M. Arundell, A. Valencia, G. Gomila, High-speed particle detection in a micro-Coulter counter with two-dimensional adjustable aperture, Biosens. Bioelectron. 24 (2008) 290–296.
[37] J. Riordon, M. Mirzaei, M. Godin, Microfluidic cell volume sensor with tunable sensitivity, Lab Chip 12 (2012) 3016–3019.
[38] J. Riordon, M. Nash, W.Y. Jing, M. Godin, Quantifying the volume of single cells continuously using a microfluidic pressure-driven trap with media exchange, Biomicrofluidics 8 (1-5) (2014) 011101.
[39] S. Yan, J. Zhang, D. Yuan, W.H. Li, Hybrid microfluidics combined with active and passive approaches for continuous cell separation, Electrophoresis 38 (2017) 238–249.